MJFAS
Malaysian Journal of Fundamental and Applied Sciences

RESEARCH ARTICLE

Stingless Bee Honey-Based Hydrogel Incorporating Plant Extracts for Wound Healing Applications

Elene Xie Yin Aw, Siti Nurhazimah Mahmud, Pg Emeroylariffion Abas, Hazwani Suhaimi*

Faculty of Integrated Technologies, Universiti Brunei Darussalam, Jalan Tungku Link, Gadong BE1410, Brunei

Abstract Hydrogels are solid-like materials that are widely used in medicine, particularly as wound dressings, due to their ability to retain moisture, protect wounds from external contaminants, and remain permeable to oxygen. In this research, hydrogels were fabricated using chitosan, pectin, gelatin, stingless bee honey, and the incorporation of medicinal plant extracts to enhance their therapeutic properties. The aim of this study was to fabricate hydrogels incorporating three different medicinal plants and to evaluate their physical, chemical, mechanical, and biological characteristics, as well as to identify the most suitable medicinal plant for wound-dressing applications. FTIR analysis of hydrogel with and without plant extracts confirmed the presence of functional groups associated with the polymers, honey, and plant extracts. Swelling testing revealed a high water absorption capability and this demonstrated their ability to maintain a moist healing environment. XRD analysis exhibited amorphous structures for all samples, indicating that the addition of plant extracts did not alter their crystallinity. Mechanical testing showed that extract-loaded hydrogels exhibited Young's modulus values of 0.10-0.19 MPa compared to 0.20 MPa for the control, suggesting reduced stiffness upon extract incorporation, with Ulam Raja formulations showing the greatest reduction from 0.18 MPa to 0.10 MPa as extract loading increased. Biocompatibility assessment using human osteoblast cells showed no cytotoxic effects in all hydrogel formulations, with cell densities increasing from 6.09×10^6 cells/mL at Day 0 to 1.10×10^7-4.70×10^7 cells/mL at Day 5, under the current experimental conditions.

Keywords: hydrogel; plant extract; honey; wound healing; biocompatibility; natural polymer; phytochemical; extract loading.

Introduction

Wound healing is a coordinated and highly regulated physiological process that restores the structural and functional integrity of the skin. As the largest organ of the human body, the skin functions as a primary defence barrier against chemical, physical, and microbial insults. Damage to this barrier can lead to injury and trigger a cascade of events involving haemostasis, inflammation, proliferation, and remodelling, where each stage requires precise cellular and molecular coordination [1], [2], [3]. If these recovery processes are disturbed by infection, underlying disease or environmental stress, the healing response may become impaired and eventually cause chronic wounds that impose significant clinical and economic burdens [3]. These limitations emphasize the requirement for advanced wound dressings designed to actively support tissue regeneration instead of just providing passive coverage.

Conventional wound dressings such as gauze, plasters and bandages are primarily served as physical protection to the wound. However, their functions are limited by their incapacity to maintain an optimal moisture balance, effectively absorb exudates or prevent bacterial colonization. Additionally, their fibres may adhere to the wound surface, which can cause pain upon removal and disrupt newly formed tissue,

***For correspondence:**
hazwani.suhaimi@ubd.edu.bn

Received: 02 Apr. 2026
Accepted: 07 Jul 2026

ultimately slowing down the healing and increasing the risk of infection [4], [5]. Therefore, modern wound management has evolved toward functional biomaterials as they can enhance healing by maintaining moisture, facilitating fluid exchange and regulating the wound environmental condition [6].

Hydrogels are modern wound dressing materials that are widely recognized due to their high water content, biocompatibility, oxygen permeability and extracellular matrix-like structure [7], [8]. They possess a three-dimensional network that maintains a moist environment for cell adhesion, nutrient exchange and controlled exudate absorption. Moreover, they can act as reservoirs for bioactive molecules and control the release of therapeutic agents to the wound site [9].

Hydrogels that are composed of natural polymers such as chitosan, gelatin, and pectin provide additional benefits for biomedical applications [10], [11]. Chitosan possesses intrinsic antimicrobial and haemostatic properties due to electrostatic interactions between its protonated amino groups and negatively charged microbial membranes [12], [13]. Gelatin contains cell-adhesive motifs that enhance cell attachment and proliferation but often require crosslinking to overcome its mechanical limitations[14], [15]. Pectin can enhance the strength and biocompatibility of hydrogels through anionic carboxyl groups that engage in hydrogen bonding and ionic interactions [14], [16]. In combination with these polymers, they can form a biodegradable and bioactive matrix that is suitable for wound healing applications.

Hydrogels incorporating natural bioactive compounds have attracted increasing attention in recent years as a strategy to enhance wound healing efficacy. Among the various natural bioactive agents studied, honey has emerged as a promising candidate due to its established use in treating burns, ulcers, and infected wounds. Its antibacterial, anti-inflammatory, and antioxidant properties are attributed to hydrogen peroxide production, low pH, high osmolarity, and the presence of phenolic compounds and flavonoids [12], [17], [18], [19], [20]. Honey, particularly derived from stingless bees, showed strong antibacterial and antioxidant potential due to its high acidity and abundant phytochemical content, which collectively contribute to tissue regeneration and inhibition of microbial growth [19], [20], [21], [22], [23].

Beyond honey, medicinal plant extracts offer a promising source of bioactive additives for wound healing. Recent reviews have emphasized that incorporating such natural therapeutic agents into polymeric hydrogel matrices enhances multifunctional wound-healing performance [24]. For centuries, plant-derived therapeutics and bee products have been used to treat wounds and prevent infection. A wide range of botanicals, such as Aloe vera, Curcuma longa, Azadirachta indica, Camellia sinensis, Centella asiatica, Calendula officinalis, Matricaria chamomilla L., and Hypericum perforatum, have been widely examined for their antioxidant, anti-inflammatory, antimicrobial, and collagen-promoting activities [24]. These therapeutic effects are largely attributed to their richness in phenolics, flavonoids, tannins, alkaloids, and terpenoids that support wound healing through reducing oxidative stress, modulating inflammation, enhancing collagen synthesis, and preventing bacterial infection [25], [26]. There are several plants commonly used in Bruneian traditional medicine, such as *Melastoma malabathricum (Kuduk-Kuduk)*, *Eleutherine bulbosa (Bawang Sampar)*, and *Cosmos caudatus (Ulam Raja)*. They are particularly rich in bioactive compounds and exhibit strong antioxidant and antimicrobial activities [27], [28], [29], [30], [31], [32]. Such properties are favourable for wound healing, where the control of oxidative stress and microbial contamination plays an important role in tissue repair. Therefore, these medicinal plants are specifically selected for incorporation into the hydrogel system. Integrating these plant extracts into hydrogel matrices offers a sustainable and culturally relevant approach to developing multifunctional wound dressings.

Despite the promising therapeutic potential of hydrogels, the incorporation of region-specific medicinal plant extracts into honey-based polysaccharide hydrogels remains underexplored, particularly in the context of stingless bee honey. While honey- and plant extract-based hydrogel systems have been previously reported, existing studies are predominantly focused on Apis-derived honey and individual formulations, with limited systematic comparison of multiple bioactive additives within a consistent polymer matrix. The rich biodiversity of Brunei remains an underexploited source of natural bioactive compounds that may be harnessed to enhance hydrogel performance and support the development of local biomedical innovation. Therefore, this study focuses on fabricating and characterizing novel composite hydrogels formulated from chitosan, gelatin, pectin, stingless bee honey, and carefully selected local medicinal plant extracts. The hydrogel is analyzed through physicochemical, mechanical, and biological analyses, which include Fourier Transform Infrared Spectroscopy (FTIR) profiling, swelling testing, X-ray Diffraction (XRD) evaluation, tensile testing, and biocompatibility assessment. For the biological evaluation, both two-dimensional (2D) and three-dimensional (3D) culture systems were employed in this study. Generally, a 2D culture system provides a useful baseline for cellular behavior, whereas a 3D culture system more closely resembles the cellular environment in vivo. Therefore, comparing these two culture systems provides valuable insights into the biocompatibility assessment of

the developed hydrogels. This study adopts an exploratory, comparative framework to investigate how the incorporation of selected local medicinal plant extracts influences the structure and properties of honey-based hydrogels, thereby establishing composition–property–biological response relationships within this composite system and assessing its potential applicability in natural-based wound dressing applications.

Materials and Methods

Materials

Both chitosan and glacial acetic acid were obtained from a commercial supplier in Malaysia. Both pectin and bovine gelatin were purchased from a local grocery store in Brunei. Food-grade pectin and bovine gelatin were used in this exploratory comparative study, with the same material sources and grades maintained across all formulations to ensure consistency of the base hydrogel matrix. Raw stingless bee honey, particularly from the local Heterotrigona itama stingless bee species, was sourced locally. Absolute ethanol, reverse osmosis (RO) water, phosphate-buffered saline (PBS), Dulbecco's Modified Eagle Medium (DMEM), Human Osteoblast (HOB) cells, and Trypan blue dye were purchased from Sigma-Aldrich (Singapore). Unless otherwise stated, the solvents and reagents used were of analytical grade and were used directly in laboratory work without any further purification.

Plant Extraction

Fresh *Melastoma malabathricum (Kuduk-Kuduk)* flowers, *Cosmos caudatus (Ulam Raja)* leaves, and *Eleutherine bulbosa (Bawang Sampar)* bulbs were collected from Panaga, Seria, in Daerah Belait, Brunei Darussalam. The plants were washed several times with tap water to remove all dirt and surface impurities. The cleaned plants were then dried using a food dehydrator at 65°C for about 4 to 5 hours to achieve consistent moisture removal. After the plants were dried, they were crushed by a mortar and pestle and sieved with a stainless-steel flour sifter to obtain a uniform particle size. Each of the powdered plant samples was stored in a sealed plastic container at room temperature for further use.

A total of 10 g of a powdered sample of a certain type of plant was added to 100 mL of 70% ethanol (1:10 w/v ratio) and then heated at 45°C under magnetic stirring at 800 rpm for an hour. During the ethanolic extraction, the beaker was covered with a lid to prevent solvent evaporation and maintain stable extraction conditions. The macerated mixture was vacuum-filtered using Whatman filter paper No. 3 to separate the solid residues from the ethanolic extracts. The filtrate was then left to evaporate on a hotplate at 45°C to remove most of the ethanol up to 20mL and obtain a 0.5g/mL of concentrated crude extract. The concentrated extract was transferred into an airtight container and preserved in the refrigerator. The maceration steps were performed again for the other two types of plants.

It should be noted that the plant extracts employed in this study were crude ethanolic extracts without further fractionation. The exact chemical composition of these extracts was not characterized and may vary depending on extraction parameters and storage conditions. Therefore, any observed effects on formulated hydrogel properties and biocompatibility are interpreted at the formulation level, and further studies would enable detailed characterization of the extract composition.

Hydrogel Fabrication

Hydrogels were formulated using chitosan, pectin, gelatin, stingless bee honey, and various types and amounts of plant extract. A 40 mL volume of raw honey was maintained, as it was the optimal volume found in one of the studies [1]. The volume of plant extract was varied to analyse its effect on the hydrogel's properties. Hydrogels were prepared with 0 mL (control), 1 mL, 5 mL and 9 mL of plant extract, as shown in Table 1. Since there were three types of plant extract, 10 different hydrogels were synthesized. For each hydrogel sample, the total volume of the solution was maintained at 120 mL by adjusting the volume of RO water. This ensures all samples had an identical polymer-to-solvent ratio.

Table 1. Composition of polymers, honey and plant extracts prepared for hydrogel formulation.

Hydrogel sample number	Volume of honey (mL)	Volume of RO water (mL)	Volume of plant extract (mL)	Volume of chitosan solution (mL)	Mass of gelatin powder (g)	Mass of pectin powder (g)
1	40	70	0	10	2.5	5
2	40	69	1	10	2.5	5
3	40	65	5	10	2.5	5
4	40	61	9	10	2.5	5

To prepare the chitosan solution, 1 g of chitosan powder was dissolved in 100 mL of 1% (v/v) acetic acid. The mixture was heated and continuously stirred on a magnetic hot plate to facilitate complete dissolution, as chitosan requires a mildly acidic environment for the protonation of its amino groups.

For the polymer blend, RO water was first measured according to each formulation (for example, 70 mL for the control hydrogel). 5g of pectin powder was gradually added to the water under constant stirring until fully dispersed. 2.5g of gelatin powder was then added to the solution and allowed to dissolve completely. Subsequently, 10 mL of the prepared chitosan solution (containing 0.1 g of dissolved chitosan) was added to the polymer mixture.

The 40 mL of stingless bee honey was incorporated next, followed by the addition of plant extract according to the designated volume (0, 1, 5, or 9 mL). RO water was then added up to the overall amount of 120 mL. The mixture was stirred thoroughly until a homogeneous solution was achieved.

To remove air bubbles that formed during the mixing process, the resulting hydrogel solutions were subjected to ultrasonication for 10 minutes at 60% amplitude, using a 1-second on and 1-second off pulsing cycle. Degassing was a crucial process to prevent pore irregularities that could occur in hydrogels during solidification, which could affect the mechanical integrity and uniformity of the hydrogel films.

A degassed hydrogel solution was cast onto petri dishes with a thickness of 2 mm. The cast hydrogel films were oven-dried at 40°C for 24 hours to remove the moisture and allow them to solidify. After the hydrogels solidified, the films were carefully peeled from the petri dishes and air-dried at room temperature for five days to further stabilize the hydrogel matrix. The hydrogel was formed through physical interactions without the use of chemical crosslinking agents.

Characterization Techniques

Functional Group Analysis

The chemical structure of hydrogel with and without the addition of plant extracts was characterized using a Shimadzu IRAffinity-1 FTIR spectrophotometer (Shimadzu Corporation, Kyoto, Japan). The air-dried hydrogels were cut into small pieces and placed directly onto the sample holder of the FTIR. Spectral data were collected in the transmission mode within the range of 4000 cm^{-1} to 400 cm^{-1}, using a resolution of 4 cm^{-1} and 32 scans per sample. The obtained data were used to identify functional groups and confirm the presence of characteristic chemical bonds within the hydrogel structure.

Swelling Analysis

Air-dried hydrogel samples were initially weighed to obtain their dry mass (W_{dry}). The samples were then immersed in 2 mL of PBS at pH 7.4, which provides a controlled and reproducible aqueous environment for the swelling test, while noting that PBS does not fully replicate the ionic composition of wound exudate. The hydrogels in beakers were maintained at 37°C, which is near to human physiological temperature. At regular time intervals, the PBS were removed and the beakers containing the swollen hydrogels were weighed to obtain the wet mass (W_{wet}). Prior to the swelling test, the used beaker was pre-weighed to ensure accurate calculations.

Swelling degree, D_s, is used to measure the average degree of crosslinking and it is evaluated using Equation (1):

$$D_s = \frac{W_{wet} - W_{dry}}{W_{dry}} \times 100\% \quad (1)$$

This parameter represents the hydrogel's capacity to absorb and retain moisture. Thus, a higher D_s value indicates a higher water holding ability, which is beneficial for preventing wound dehydration and promoting a favorable healing environment [1].

Crystallinity Analysis

XRD analysis was conducted to examine and compare the crystalline structures of the hydrogels with and without plant extract using an Aeries benchtop X-ray diffractometer. Before analysis, the air-dried hydrogel films were cut into regular shapes and fit properly onto the sample holder. Diffraction patterns were recorded over a 2θ range of 10° to 80°. The X-ray generator was operated at 40 kV and 15 mA, with a scanning speed of 10° per minute and a step size of 0.02°. Diffraction patterns were recorded over a 2θ range of 10° to 80°, and the resulting patterns can be used to determine the crystallinity of hydrogels.

Tensile Strength Analysis

The mechanical strength of the hydrogels with and without plant extract was examined using an AMETEK LLOYD LS100PLUS universal testing machine fitted with a 5kN load cell and 5kN grips. Rectangular hydrogel strips, measuring 8 cm in length and 1 cm in width, were prepared and placed between the grips. Samples were stretched at an extension rate of 2 mm/min, and the applied force and corresponding extension were continuously recorded using NEXYGEN software. The stress-strain curve can be obtained from the test, and the curve can be used to determine the Young's modulus of the hydrogels. This analysis helps assess the ability of hydrogels to endure mechanical stress, which is essential for their performance as wound dressing materials.

Cell Viability and Cytoxicity Analysis

Experimental Setup

For the biocompatibility assessment, the experiment was carried out for five days using a 24-well culture plate with five different setups: a 2D culture system and four 3D systems with Kuduk-Kuduk (KK), Ulam Raja (UR), Bawang Sampar (BS), and control (CC) hydrogels. In the 3D systems, the culture medium consists of both the hydrogel matrix and the seeded cells, whereas the 2D system contains only the culture medium and cells. The 2D culture was used as a control to represent normal cell behaviour in the absence of a hydrogel. Any differences in cell growth observed in the 3D culture systems could therefore be related to the hydrogel environment rather than to the cells themselves. Manual cell counting was performed on samples collected from the respective wells at the end of days 1, 3, and 5 of the culture periods [33].

Hydrogel Sterilization

Before cell seeding, hydrogels were sterilized by immersing them in 70% ethanol for 10 minutes and subsequently rinsing twice with phosphate-buffered saline (PBS) to remove any residual ethanol. This procedure ensures effective sterilization and reduces the likelihood of contamination during cell culture.

Cell Culture and Seeding

Supplemented Dulbecco's Modified Eagle Medium (DMEM) was pre-warmed at 37°C, and the frozen HOB vial was rapidly thawed in a 37°C water bath until fully liquefied. After surface sterilization, the thawed cells were transferred into pre-warmed medium and centrifuged. The resulting cell pellet was resuspended in fresh medium within a T-75 flask and incubated at 37°C with 5% CO_2 and 95% air for four to five days. Prior to cell seeding, all hydrogels were sterilized to prevent microbial contamination. For the 3D culture setup, each hydrogel sample was cut into circular shapes approximately 1 cm in diameter, where 1 mL of HOB cell suspension (6.09×10^6 cells per well) was seeded onto each hydrogel in a 24-well plate, while control wells (2D setup) received the same number of cells without hydrogels. All hydrogel samples were prepared under identical conditions to ensure consistency in composition, geometry, and handling across all experimental groups.

Cell Proliferation Assay

HOB cells were seeded onto sterile square-shaped sections of the composite hydrogels placed in a 24-well plate to establish the 3D culture. At predetermined intervals, the culture medium from each well on the plate was collected and mixed with an equal volume of 0.1% (w/v) trypan blue solution. Trypan blue dye was used to differentiate viable cells from non-viable cells by observing the stained samples under a light microscope on a hemocytometer. Cell growth and viability were manually monitored at 24, 72, and 120 hours (days 1, 3, and 5) [33].

Trypan Blue Assay

For each time point (days 1, 3, and 5), an equal volume of the cell suspension and trypan blue dye was combined in a centrifuge tube to allow uniform staining for manual cell counting. The stained mixture

was then loaded onto a hemocytometer and covered with a cover slip over the counting chamber to achieve proper capillary filling. After that, the hemocytometer was placed on the microscope stage, and the cells were counted within the middle square and the four corner squares of the grid to ensure representative sampling [34]. It should be noted that the cell culture experiments were conducted as a single experimental set for both the 2D and 3D culture systems; Therefore, the results are interpreted within a comparative framework, focusing on formulation-dependent trends in cellular response across different hydrogel systems under consistent experimental conditions. In this assay, viable cells excluded the dye and appeared clear, whereas non-viable cells absorbed the dye and appeared blue. Cell concentration and viability were subsequently calculated using Equations (2)-(5) [33].

Cell viability was calculated according to the formula presented in Equation (2):

$$Viable\ cells\ (\%) = \frac{Number\ of\ viable\ cells}{Total\ number\ of\ cells} \times 100 \quad (2)$$

The average viable cell count per square was derived using Equation (3):

$$Average\ viable\ cells\ per\ square = \frac{Number\ of\ viable\ cells}{Number\ of\ squares\ counted} \quad (3)$$

To account for sample dilution during staining, the dilution factor was computed based on the ratio of the combined cell-dye mixture volume to the original cell suspension volume, as shown in Equation (4):

$$Dilution\ factor = \frac{Total\ volume\ of\ cell{-}dye\ mixture}{Volume\ of\ cells} \quad (4)$$

Lastly, Equation (5) was applied to determine the viable cell concentration (cells/mL) in the original sample:

$$Cell\ concentration\ \left(\frac{viable\ cells}{mL}\right) = Average\ viable\ cells\ per\ square \times Dilution\ factor \times 10^4 \quad (5)$$

The factor of 10^4 is used because each counting square on the hemocytometer represents a volume of 0.0001 mL [33].

Results and Discussion

Visual Appearance of the Fabricated Hydrogels

Figure 1 shows the images of the fabricated hydrogels. It can be seen that the hydrogels have a homogeneous appearance and were easily removed from the petri dishes without visible structural failure, confirming successful solid-like hydrogel formation.

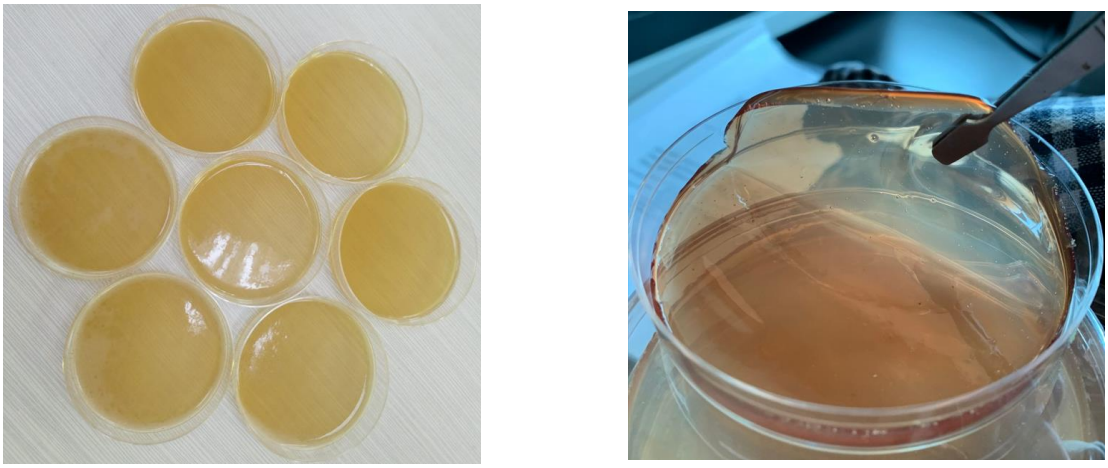

(a) (b)

Figure 1. Representative images of the fabricated hydrogels: (a) formed hydrogels in petri dishes and (b) hydrogel film.

FTIR Analysis

FTIR spectra of the hydrogels were analysed by identifying the characteristic regions associated with the functional groups present in polysaccharides, proteins, and plant-derived compounds. The broad absorption located within the 3200-3600 cm^{-1} region is attributed to the O-H and N-H stretching vibrations, which reflects the hydroxyl groups of pectin, chitosan, honey, and polyphenolic constituents of the plant extracts, as well as amide groups of gelatins. The band observed in the 2700-3000 cm^{-1} region is associated with aliphatic C-H stretching of $-CH_2$ and $-CH_3$ groups. The spectral region between 1600-1800 cm^{-1} corresponds to C=O stretching, including ester carbonyls from methyl-esterified pectin, together with the amide I band of gelatin. The 1200–1500 cm^{-1} fingerprint region contains characteristic carboxylate signals and the amide III band located between 1220–1300 cm^{-1}, arising from C–N stretching and N–H bending. Strong absorptions in the 900–1100 cm^{-1} range correspond to glycosidic C–O stretching.

Figure 2(a) illustrates the FTIR spectra of the hydrogels containing 1 mL extract. A broad absorption observed at ~ 3275 cm^{-1} corresponds to O–H stretching vibrations. The aliphatic C–H stretch at ~ 2928 cm^{-1} is present with minimal changes across all samples. At ~ 1735 cm^{-1} and ~ 1635 cm^{-1}, the ester C=O and amide I bands appear respectively. In the fingerprint region ranging from 1239–1415 cm^{-1}, slight variations in intensity for B1 and K1 were observed. The strong glycosidic C–O–C band at ~ 1019 cm^{-1} remains present in all samples.

At the 5 mL extract loading shown in Figure 2(b), the FTIR spectra show similar characteristic bands. A broad O–H and N–H stretching band near 3290 cm^{-1} appears widened with reduced transmittance in U5. The C–H stretching peak near 2921 cm^{-1} shows higher intensity in B5 and K5, which may reflect contributions from components present in the plant extracts. The ester C=O band in U5 shifts slightly to 1718 cm^{-1}, while the amide I band appears near 1635 cm^{-1} with reduced intensity. In the fingerprint region of 1229–1395 cm^{-1}, U5 exhibits band broadening and lower transmittance. The polysaccharide C–O–C band at 1023 cm^{-1} remains evident.

For Figure 2(c), the FTIR spectra at 9 mL also demonstrate the presence of the functional groups. The O–H and N–H stretching region at 3275 cm^{-1} shows markedly lower transmittance in U9. In B9 and K9, minor shifts in the aliphatic C-H band at ~ 2914 cm^{-1} were observed. The ester C=O and amide I bands remain visible at approximately 1705 cm^{-1} and 1635 cm^{-1} with reduced intensity. In the fingerprint region spanning 1231–1372 cm^{-1}, U9 exhibits marked suppression and peak broadening. The polysaccharide C–O–C stretching band at ~ 1015 cm^{-1} remains present.

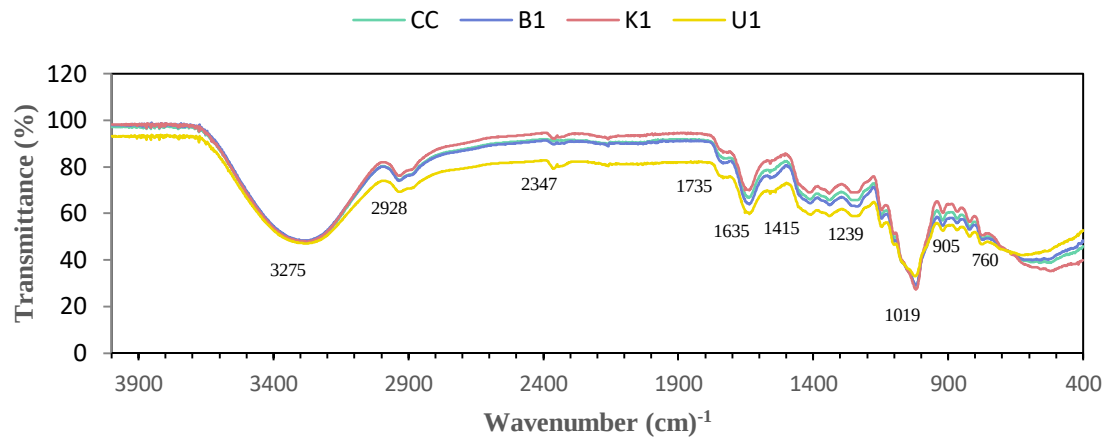

(a)

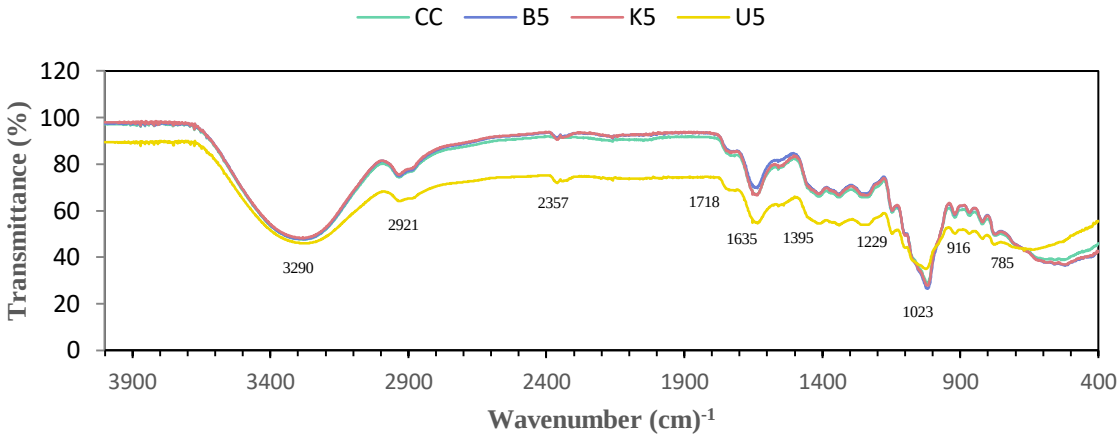

(b)

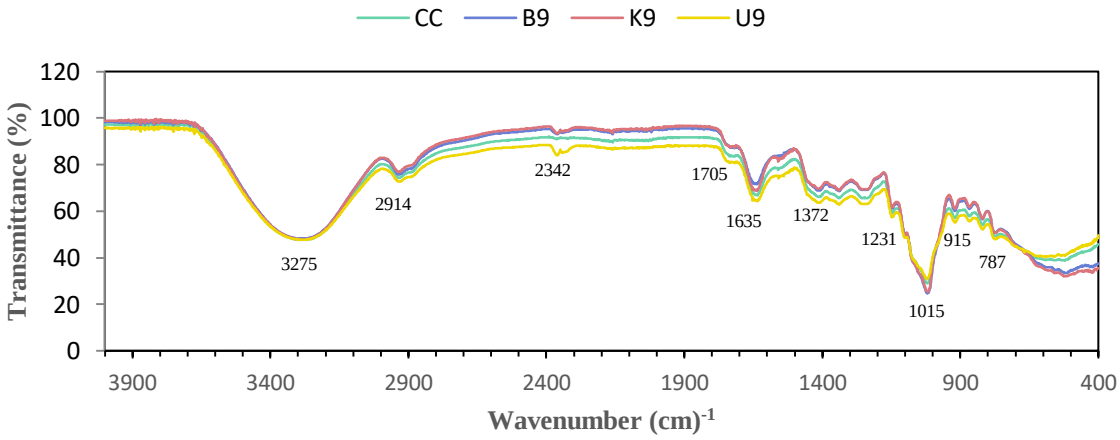

(c)

Figure 2. FTIR spectra of composite hydrogels with and without plant extracts at varying concentrations: (a) 1 mL extract, (b) 5 mL extract, and (c) 9 mL extract.

Swelling Test Analysis

The swelling behaviour of hydrogels incorporating various plant extract types and concentrations is presented in Figure 3 through an approximation procedure that tracks changes in swelling over the experimental duration. Samples were grouped according to extract concentrations (1 mL, 5 mL, and 9 mL) and further classified according to extract types, namely Kuduk-Kuduk (K-series), Bawang Sampar (B-series), and Ulam Raja (U-series). Curve approximation was used to visually illustrate the general swelling trends over the experimental duration. This graphical representation allows for direct comparison between formulations. It is particularly useful for identifying concentration-dependent reductions in swelling as well as differences associated with each plant extract. High R^2 values confirm a strong correlation between the experimental data and the selected mathematical models. This supports the reliability of the swelling behavior.

In Figure 3, the swelling behaviour of all hydrogel samples were followed by a polynomial (quadratic) swelling model instead of an exponential decay trend. The high R^2 values ranging from 0.86 to 0.95 confirm the reliability of this fitting approach.

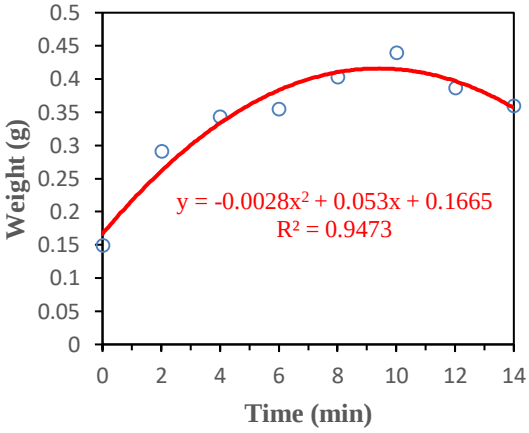

(a)

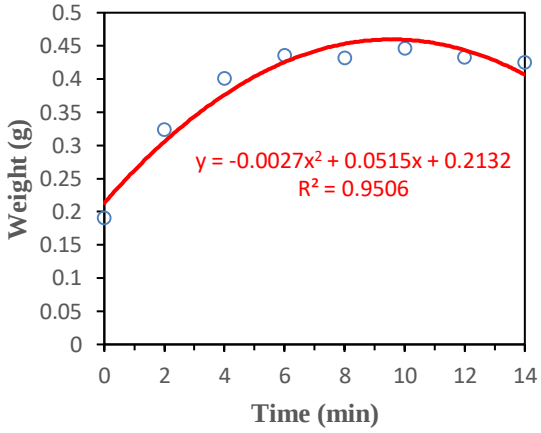

(b)

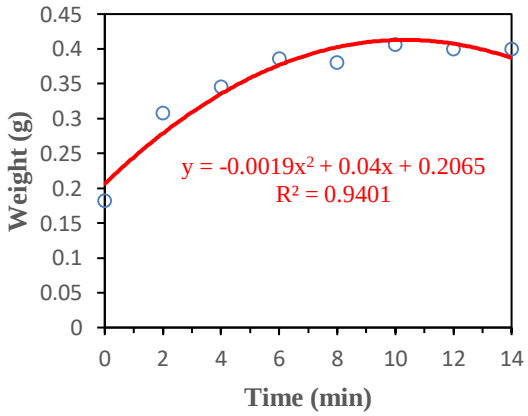

(c)

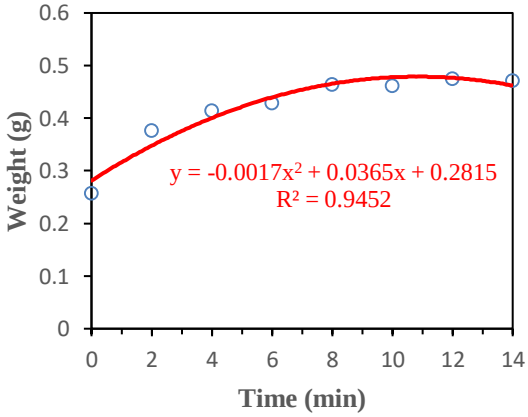

(d)

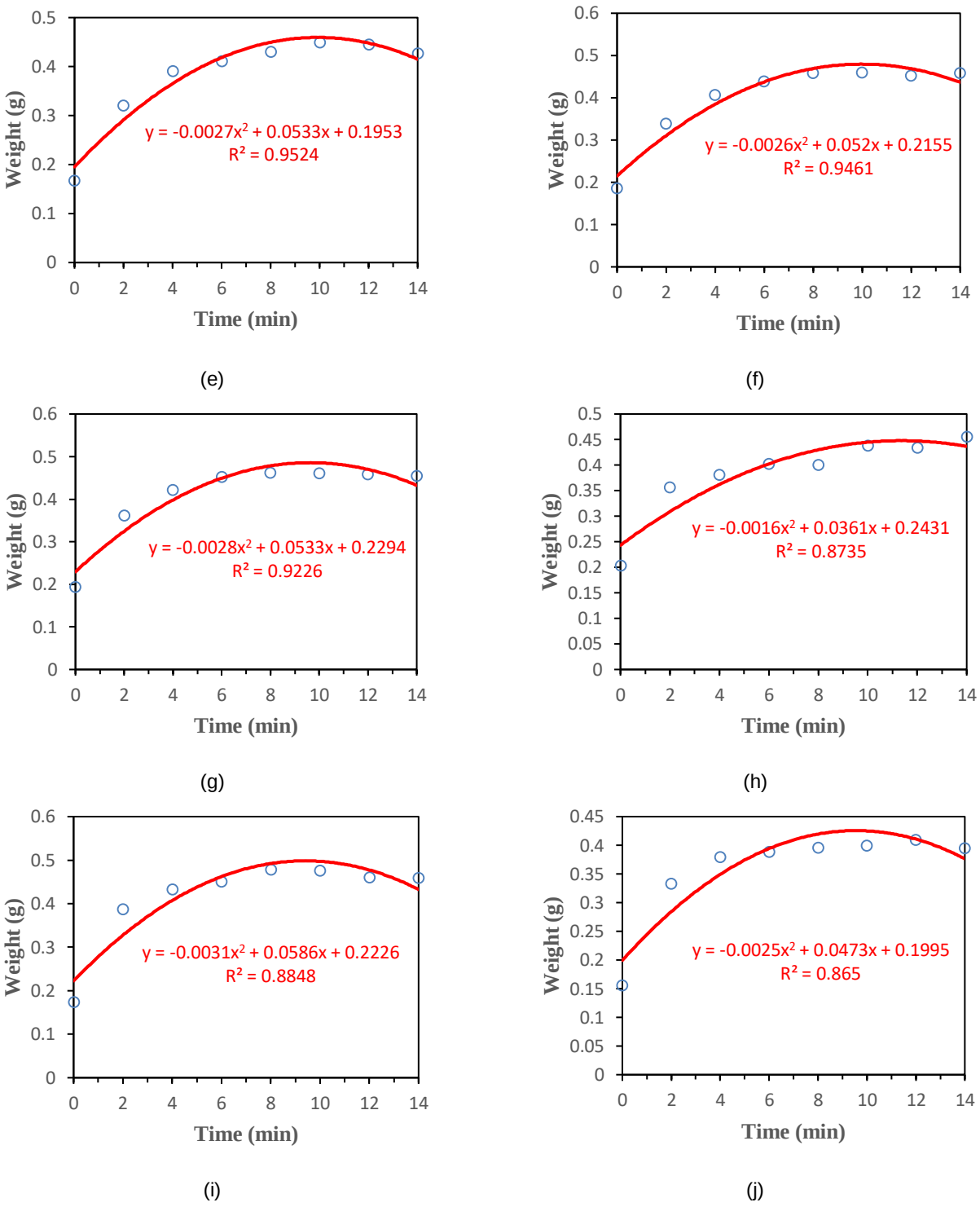

Figure 3. Time-dependent changes in the weight of the hydrogels during the swelling test: (a) CC hydrogel, (b) B1 hydrogel, (c) B5 hydrogel, (d) B9 hydrogel, (e) K1 hydrogel, (f) K5 hydrogel, (g) K9 hydrogel, (h) U1 hydrogel, (i) U5 hydrogel, and (j) U9 hydrogel.

A parabolic trend was observed in the swelling behaviour of the hydrogels, which is consistent with swelling dynamics reported for similar biopolymer-based dressings [1]. At the initial stage of immersion, all samples presented a rapid increase in mass because of the capacity of physically crosslinked hydrogels to dissolve in water. This initial swelling phase is governed by the presence of numerous hydrophilic functional groups like –OH, –COOH, or –NH that originate from chitosan, pectin, gelatin, and

honey, which readily attract water molecules and facilitate fast fluid penetration into the polymer network. At this stage, some polymer chains start to dissolve, but the mass increases from water uptake dominates. With continued immersion, some loosely bound polymer chains continue to dissolve and thereby reducing the hydrogel mass. The rate of water uptake also reduced as the hydrogel network became hydrated, which decreased the chain mobility and increased the internal diffusion resistance.

Among hydrogels, the CC hydrogel showed the highest swelling capacity as it has lower structural cohesion and greater susceptibility to partial dissolution. As the hydrogels are stabilized primarily by physical forces, swelling is intrinsically coupled with partial dissolution of the network or its components. In contrast, extract-loaded hydrogels from the B-series, K-series, and U-series exhibited a concentration-dependent reduction in apparent swelling. The presence of plant extract may contribute to interactions within the hydrogel network. Phytochemical constituents such as polyphenols, flavonoids, tannins, and organic acids are capable of forming hydrogen bonds or other secondary interactions with the hydrogel components, thereby tightening the network structure and reducing pore accessibility. Variations in swelling reduction across the extracts reflect the differences in their phytochemical richness. For instance, K-series hydrogels generally showed the highest swelling reduction, likely due to their high phenolic and tannin content of *Melastoma malabathricum,* which promotes crosslinking within the polymer network. The U-series exhibited moderate swelling suppression that corresponds to the flavonoid-dominant composition of *Ulam Raja*, whereas the B-series hydrogels showed the lowest swelling reduction which indicates weaker interactions between *Eleutherine bulbosa* constituents and the polymer matrix. However, this interpretation requires further examination of the interaction between plant extracts and the hydrogel matrix.

At low extract loading of 1 mL, the reduction in swelling was minimal, suggesting that water uptake and partial dissolution of the hydrogel network mostly govern the swelling behaviour. However, at concentrations of 5 mL and 9 mL, the swelling ratios decreased more noticeably. As per reference [35], the introduction of plant additives may alter both the chemical and physical structure of the hydrogel matrix, with these additives potentially interacting with the polymer network, and hence, increasing or decreasing porosity depending on the intensity of the interactions. However, it should be noted that the swelling profiles primarily reflect the balance between water uptake and partial dissolution of hydrogels, and do not provide quantitative information on macromolecular interactions. Therefore, while reduced swelling was observed at elevated extract loading, this may indicate the formation of a relatively denser network or reduced pore accessibility within the hydrogel matrix; this interpretation remains qualitative, and further studies would enable detailed elucidation of the underlying interaction mechanisms. Nevertheless, the observed concentration-dependent modulation of water absorption remains relevant for wound healing applications, where balanced fluid regulation is essential for maintaining a favorable healing environment.

XRD Analysis

The XRD patterns of the hydrogel without plant extracts and the hydrogels containing 1 mL, 5 mL, and 9 mL of plant extracts are shown in Figure 4. The XRD results demonstrate that all samples exhibit a predominantly amorphous structure. In the figure, the observed diffraction profiles are characterized by a single broad halo centred at 2θ between 30° and 35°, with no sharp or well-defined crystalline peaks [36]. These broad, diffuse X-ray diffraction peak patterns indicate the lack of highly ordered and long-range crystalline structure. The similarity of the broad patterns across all plant extract types and concentrations suggests that no detectable crystalline domains, including those potentially arising from honey crystallisation, were present within the hydrogel matrix.

The lack of crystalline domains in the hydrogel structure is generally considered favorable for biomedical and controlled-release applications. In an amorphous structure, the disordered molecular arrangement allows greater molecular mobility within the network compared to crystalline forms, which can promote dissolution. This amorphous phase may contribute to more uniform swelling behaviour and support controlled or sustained release of bioactive compounds [36], [37].

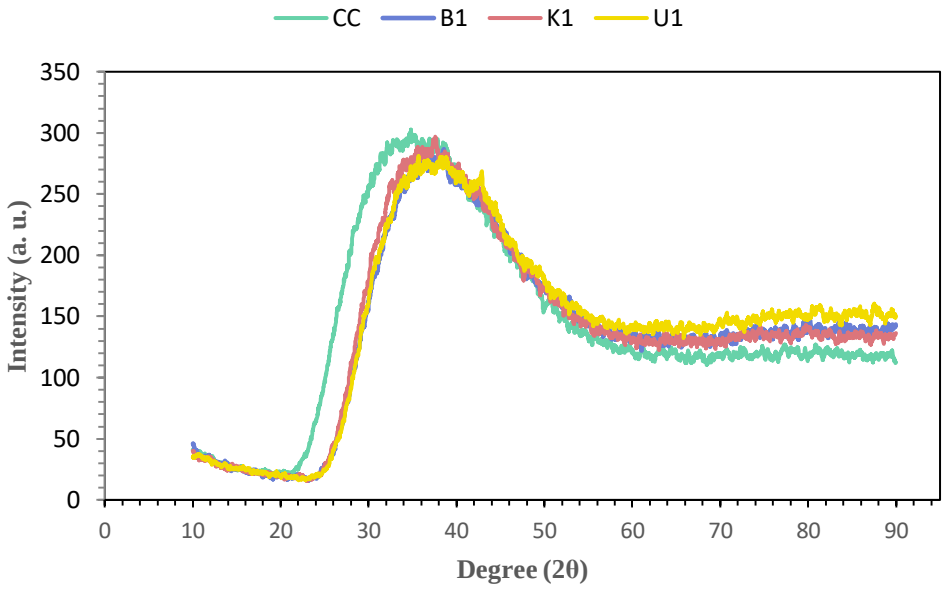
CC
B1
K1
U1
Intensity (a. u.)
Degree (2θ)
0
50
100
150
200
250
300
350
0
10
20
30
40
50
60
70
80
90

(a)

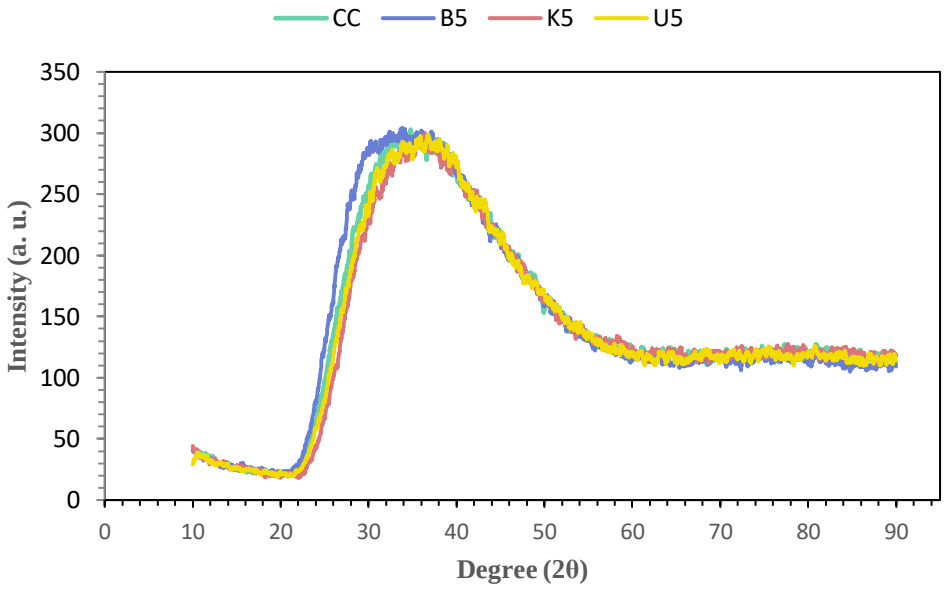
CC
B5
K5
U5
Intensity (a. u.)
Degree (2θ)
0
50
100
150
200
250
300
350
0
10
20
30
40
50
60
70
80
90

(b)

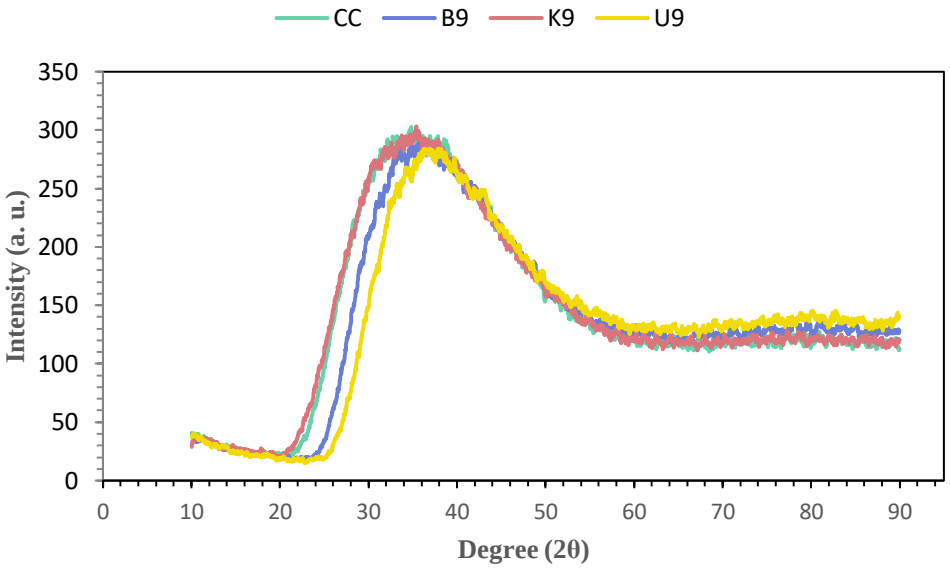

(c)

Figure 4. XRD spectra of composite hydrogel with: (a) 1 mL, (b) 5 mL, and (c) 9 mL extract, and with CC as control reference.

Tensile Test Analysis

As presented in Figure 5, the average Young's modulus of the control and extract-loaded hydrogels exhibited distinct variations in stiffness with the incorporation of different types and volumes of plant extracts. The modulus values were measured within the initial linear range of 0-50% strain. For B-formulations, the mechanical strength was nearly identical to that of the control at lower extract levels. B1 and B5 had a modulus of approximately 0.19 MPa, which were close to the control value of around 0.20 MPa. This suggests that small amounts of Bawang Sampar did not significantly alter the hydrogel's stiffness. However, a slight reduction was observed in B9 with approximately 0.14 MPa, indicating that a higher extract content corresponds with a decrease in Young's modulus.

K-hydrogels displayed an opposite trend compared to the B-hydrogels. Both K1 and K5 exhibited reduced stiffness at approximately 0.16 MPa, and this showed a weaker strength compared to the control hydrogel. On the other hand, K9 had a value of approximately 0.18 MPa, which was closer to the stiffness of the control. It can be concluded that at higher extract loadings, Kuduk-Kuduk exhibited greater mechanical strength.

As illustrated in the figure, the U-hydrogels showed the strongest concentration-dependent weakening, indicating a high sensitivity of their mechanical properties to extract loading. At low extract loading, U1 exhibited a Young's modulus of 0.18 MPa that showed a similarity to the control and indicated minimal impact on hydrogel stiffness. However, U5 showed a significant decline to 0.12 MPa, while a further decrease to 0.10 MPa was observed for U9. This progressive decline in modulus with increasing extract volume indicates that Ulam Raja had a greater effect on the strength of the hydrogels than other extracts.

The tensile behavior observed may be linked to differences in how each plant extract distributes within the hydrogel matrix; however, further rheological and structural analyses would enable elucidation of the underlying mechanisms. Plant extracts contain their own unique compositions of bioactive compounds that may differentially affect the internal structure of the hydrogel. Some natural compounds may not disperse uniformly, which may affect the polymer chain packing. Certain hydrophobic or phenolic constituents are particularly prone to this behavior by interacting with the polymer chains and reducing overall material stiffness [37]. A pronounced reduction in stiffness was observed in the Ulam Raja hydrogels at higher extract loadings. Conversely, only minor changes were detected in the B- and K-formulations at lower concentrations, suggesting that the stiffness was less affected.

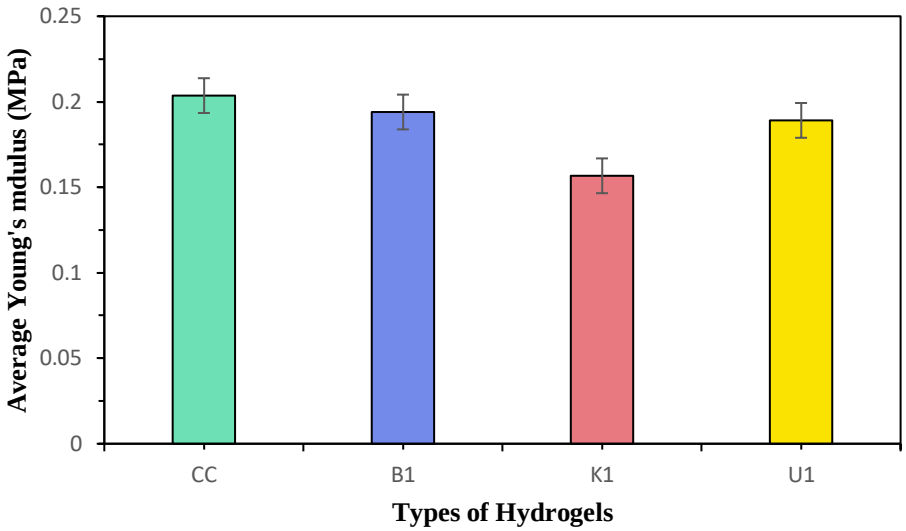
0.25
0.2
0.15
0.1
0.05
0
Average Young's mdulus (MPa)
CC
B1
K1
U1
Types of Hydrogels

(a)

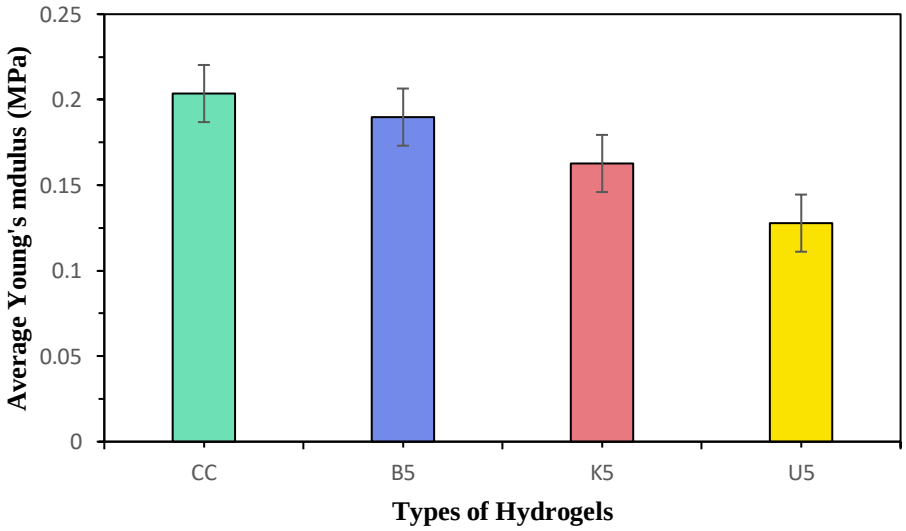
0.25
0.2
0.15
0.1
0.05
0
Average Young's mdulus (MPa)
CC
B5
K5
U5
Types of Hydrogels

(b)

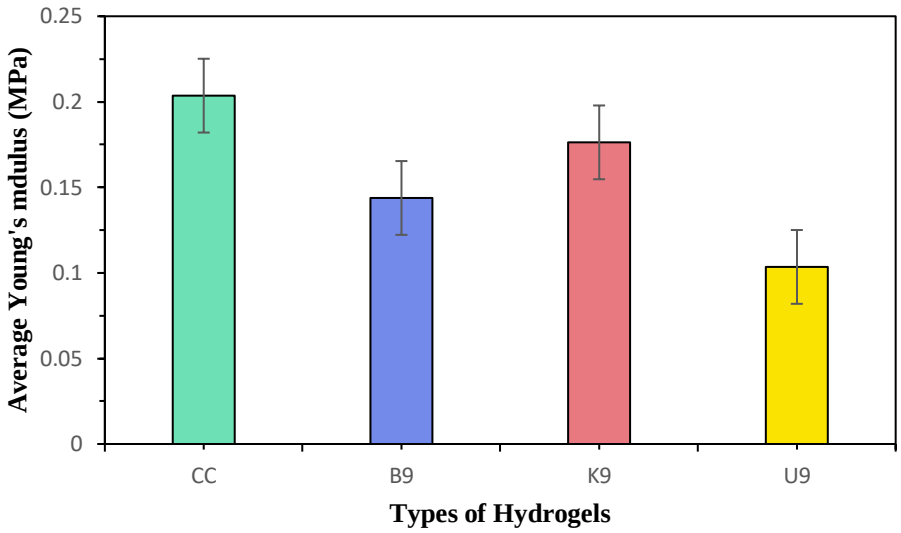

(c)

Figure 5. Average Young's modulus of hydrogels that contain different volumes of plant extract: (a) 1 mL formulations, (b) 5 mL formulations, and (c) 9 mL formulations.

Biocompatibility Analysis

Figure 6 presents the cell density profiles for the 2D control, 3D control hydrogel, and extract-loaded hydrogels, including the B-series, K-series, and U-series, across the five-day culture period. At Day 0, all samples had the same initial cell density of 6.09×10^6 cells/mL. Cell numbers increased consistently in all samples throughout the culture period. This trend suggests that the hydrogels were non-cytotoxic under the current experimental conditions and supported healthy cell growth.

As shown in Figure 6(a), progressive increases in cell density were observed in hydrogel formulations containing 1 mL of plant extract. On Day 1, B1 recorded 9.82×10^6 cells/mL, while K1 displayed a higher value of 1.05×10^7. However, U1 began more slowly at 5.60×10^6. By Day 3, all samples exhibited a substantial increase, with B1 at 2.89×10^7, K1 at 3.27×10^7, and U1 at 2.28×10^7. At the final time point, B1 declined slightly to 2.04×10^7, whereas K1 and U1 continued rising to 3.11×10^7 and 3.15×10^7. Among the three, U1 recorded the highest cell density by Day 5, while K1 maintained consistent expansion from the start of the experiment. These trends suggest that low extract concentrations supported cell growth and survival within the hydrogel matrix.

Figure 6(b) illustrates continued increases in cell density when 5 mL of extract was incorporated. On Day 1, B5 displayed the largest early increase at 1.11×10^7 cells/mL, followed by K5 at 9.37×10^6 and U5 at 6.46×10^6. The upward trend continued on Day 3, when B5 and K5 both approached 2.8×10^7 cells, whereas U5 rose to 1.40×10^7. By Day 5, clear differentiation in cell density was observed among the samples. K5 reached 4.70×10^7, the highest value across all hydrogels. B5 progressed to 3.37×10^7, while U5 increased only slightly to 1.44×10^7. This observed trend suggests that moderate incorporation of plant extracts may influence cellular expansion differently depending on the extract type.

Figure 6(c) displays more variable growth behavior at the 9 mL extract level. On Day 1, B9 and K9 recorded similar values at 7.37×10^6 and 7.98×10^6 cells/mL, while U9 remained lower at 3.88×10^6. By Day 3, B9 exhibited a sharp rise to 3.20×10^7, U9 climbed to 2.44×10^7, and K9 declined slightly to 6.80×10^6. At Day 5, B9 continued its upward trajectory, reaching 4.33×10^7. U9 fell to 1.33×10^7 and K9 rose modestly to 1.10×10^7. These results suggest that B9 showed higher observed cell densities at the highest extract volume, whereas K9 and U9 showed more variable growth profiles under the current experimental conditions.

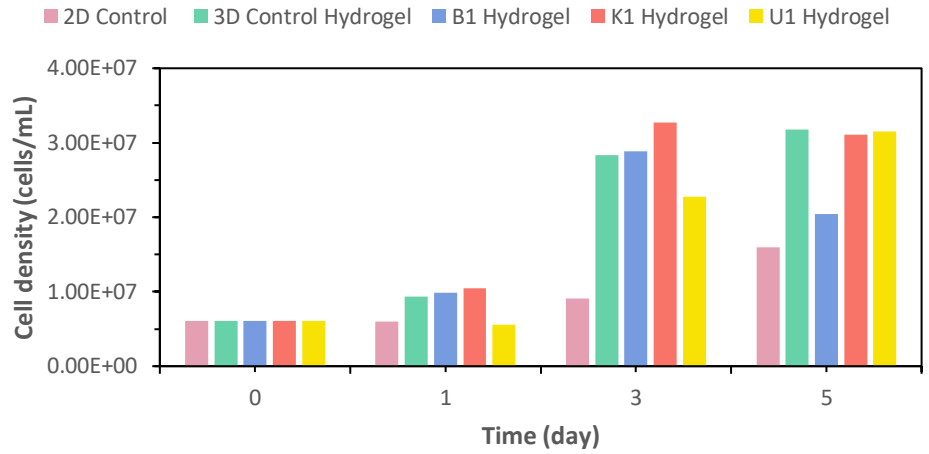

(a)

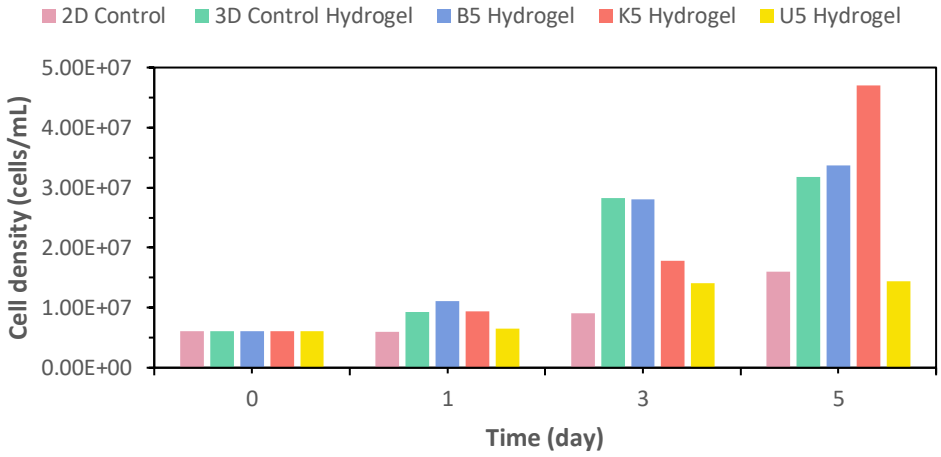

(b)

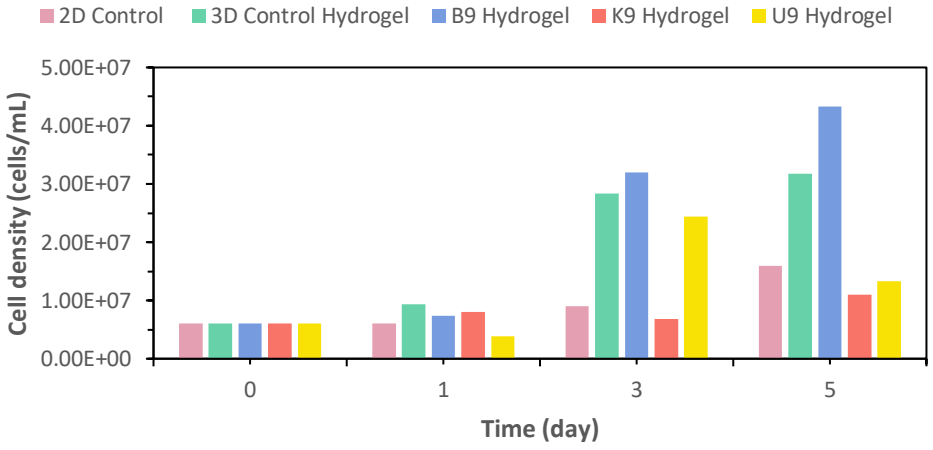

(c)

Figure 6. Five-day cell density profiles of hydrogels containing: (a) 1 mL, (b) 5 mL, and (c) 9 mL of plant extract, with 2D and 3D controls included for comparison.

The 2D control exhibited stable and predictable cell growth, providing a baseline for comparison with the 3D hydrogel systems. Among the hydrogel groups, the control composite hydrogel (CC) supported cell expansion comparable to the 2D control, suggesting that the chitosan–pectin–gelatin–honey matrix itself was compatible with osteoblast survival.

In general, the results indicate that cell proliferation trends may be influenced by the extract type and loading volume. Kuduk-Kuduk and Bawang Sampar hydrogels generally showed higher observed cell densities than Ulam Raja hydrogels under the current experimental conditions. These outcomes suggest that plant extract incorporation may influence cellular responses in honey-based hydrogel systems. As this study is designed as an exploratory, comparative evaluation of multiple formulations within a consistent hydrogel matrix, the findings should be interpreted as preliminary trends rather than definitive performance differences. Further studies incorporating replicate experiments and statistical analyses are necessary to confirm the observed trends and establish the significance of formulation-dependent differences.

Conclusions

Honey-based hydrogels have attracted increasing interest as wound-dressing materials due to their ability to maintain a moist environment, deliver bioactive compounds, and support tissue regeneration. In this study, honey-based hydrogels with medicinal plant extracts were successfully developed and characterized to evaluate their potential as wound-dressing materials. The hydrogels were formulated using natural polymers: chitosan, pectin, and gelatin, and have demonstrated favorable physicochemical, mechanical, and biological properties; supporting their potential for clinical wound-healing applications.

FTIR and XRD analyses revealed characteristic functional groups and predominantly amorphous halos across all hydrogel formulations. The hydrogels demonstrated sufficient water absorption capacity, with the control hydrogel showing the highest swelling capacity, whereas incorporating plant extracts generally reduced swelling in a formulation-dependent manner. Mechanical characterization showed that honey-based hydrogels with plant extracts generally reduced stiffness relative to the control, with Bawang Sampar-based hydrogels exhibiting the strongest mechanical performance and Ulam Raja-based hydrogels the weakest.

None of the hydrogels showed cytotoxic effects under the current experimental conditions. Hydrogels incorporating Kuduk-Kuduk and Bawang Sampar extracts generally exhibited higher observed cell densities than hydrogels incorporating Ulam Raja. As this study adopts an exploratory, comparative framework, the results should be interpreted within the context of formulation-level trends observed across samples. In addition, as food-grade pectin and bovine gelatin were used in this study, future studies using analytical- or pharmaceutical-grade polymers are recommended to further validate the suitability of the hydrogel formulations for biomedical wound dressing applications. Future studies incorporating replicate experiments, statistical analysis, more physiologically representative swelling media, and skin-relevant cell types such as dermal fibroblasts, keratinocytes, or HaCaT cells are recommended to better evaluate the wound healing performance and clinical relevance of the developed hydrogels.

In this study, the concentrations of plant extracts were selected as a priori rather than statistically optimized; therefore, systematic concentration screening and statistical optimization approaches are necessary to arrive at a true optimal balance between biological efficacy, material stability, and biocompatibility. Additionally, future studies should focus on advanced characterization techniques, including SEM–EDX, dehydration testing, rheological tests under varied thermal conditions, such as dynamic mechanical analysis, long-term degradation analysis, antibacterial testing, and antimicrobial testing, which could provide deeper insights into microstructural uniformity, degree of dehydration, crosslinking efficiency, mechanical performance, and in situ stability. As this study focuses on cell proliferation only, future studies should include the scratch-wound assay and dorsal skinfold chamber to study cell migration and skin wound healing.

Overall, this study has demonstrated that honey-based hydrogels enriched with plant extracts possess favorable physicochemical and biological properties, making them potential candidates for wound healing. However, this does not come without challenges. As most current research is in vitro, several primary challenges remain in advancing material systems toward clinical applications, including ensuring reproducibility in large-scale production, standardizing hydrogel components, and assessing the potential impact of sterilization methods on the stability of incorporated components. Further

optimization and in vivo advanced biological validation are necessary to develop these hydrogels into next-generation natural wound dressings.

Conflicts of Interest

The authors declare that there is no conflict of interest regarding the publication of this paper.

Acknowledgment

The project was funded by the Universiti Brunei Darussalam Research Grant No. UBD/RSCH/1.3/FICBF(b)/2020/005.

References

[1] H. Suhaimi, N. Murdini, N. Shamsuddin, A. Ma'amor, and P. E. Abas, "Synthesis and Characterization of Honey-Pectin Hydrogel: Exploring Potential Applications in Wound Healing," *Malaysian Journal of Fundamental and Applied Sciences*, vol. 21, no. 2, pp. 1907–1927, Apr. 2025, doi: 10.11113/mjfas.v21n2.3907.

[2] L. Qiao *et al.*, "Antibacterial conductive self-healing hydrogel wound dressing with dual dynamic bonds promotes infected wound healing," *Bioact. Mater.*, vol. 30, pp. 129–141, Dec. 2023, doi: 10.1016/j.bioactmat.2023.07.015.

[3] A. Mallick Choudhury, S. S. Mandal, N. K. Singh, M. Sahu, and P. Maiti, "Plant-extract hydrogel for effective wound healing: Animal model studies," *Chemical Engineering Journal*, vol. 514, Jun. 2025, doi: 10.1016/j.cej.2025.163131.

[4] Y. Liu, J. Liu, A. Zhang, G. Zhao, B. Jiang, and X. Zhao, "Application prospect of Marine polysaccharide hydrogels in promoting wound healing: A review," *Carbohydr. Res.*, vol. 558, Dec. 2025, doi: 10.1016/j.carres.2025.109673.

[5] S. Dhivya, V. V. Padma, and E. Santhini, "Wound dressings – a review," *Biomedicine (Taipei).*, vol. 5, no. 4, Nov. 2024, doi: 10.37796/2211-8039.1526.

[6] A. Alberts, E. T. Moldoveanu, A. G. Niculescu, and A. M. Grumezescu, "Hydrogels for Wound Dressings: Applications in Burn Treatment and Chronic Wound Care," *Journal of Composites Science*, vol. 9, no. 3, p. 133, Mar. 2025, doi: 10.3390/jcs9030133.

[7] L. Wang, M. Zhou, T. Xu, and X. Zhang, "Multifunctional hydrogel as wound dressing for intelligent wound monitoring," *Chemical Engineering Journal*, vol. 433, Apr. 2022, doi: 10.1016/j.cej.2022.134625.

[8] M. H. Norahan, S. C. Pedroza-González, M. G. Sánchez-Salazar, M. M. Álvarez, and G. Trujillo de Santiago, "Structural and biological engineering of 3D hydrogels for wound healing," *Bioact. Mater.*, vol. 24, pp. 197–235, Jun. 2023, doi: 10.1016/j.bioactmat.2022.11.019.

[9] V. Gounden and M. Singh, "Hydrogels and Wound Healing: Current and Future Prospects," *Gels*, vol. 10, no. 1, Jan. 2024, doi: 10.3390/gels10010043.

[10] M. Krishani, W. Y. Shin, H. Suhaimi, and N. S. Sambudi, "Development of Scaffolds from Bio-Based Natural Materials for Tissue Regeneration Applications: A Review," *Gels*, vol. 9, no. 2, Feb. 2023, doi: 10.3390/gels9020100.

[11] M. Krishani, N. S. Sambudi, and H. Suhaimi, "Green Catalysts in the Synthesis of Biomaterials for Biomedical Applications," in *Sustainable Green Biomaterials As Drug Delivery Systems*, vol. 1, Springer, Cham, 2025, pp. 217–252. doi: https://doi.org/10.1007/978-3-031-79062-1_9.

[12] S. W. Chin, A. S. Azman, and J. W. Tan, "Incorporation of natural and synthetic polymers into honey hydrogel for wound healing: A review," *Health Sci. Rep.*, vol. 7, no. 7, Jul. 2024, doi: 10.1002/hsr2.2251.

[13] O. Phonrachom, P. Charoensuk, K. Kiti, N. Saichana, P. Kakumyan, and O. Suwantong, "Potential use of propolis-loaded quaternized chitosan/pectin hydrogel films as wound dressings: Preparation, characterization, antibacterial evaluation, and in vitro healing assay," *Int. J. Biol. Macromol.*, vol. 241, Jun. 2023, doi: 10.1016/j.ijbiomac.2023.124633.

[14] J. Feng *et al.*, "Preparation and evaluation of chitosan/salicylaldehyde/collagen peptide Schiff base hydrogels for wound healing," *J. Mol. Struct.*, vol. 1352, Feb. 2025, doi: 10.1016/j.molstruc.2025.144554.

[15] A. Chetouani *et al.*, "Multifunctional hydrogels based on oxidized pectin and gelatin for wound healing improvement," *Int. J. Biol. Macromol.*, vol. 212, pp. 248–256, Jul. 2022, doi: 10.1016/j.ijbiomac.2022.05.082.

[16] S. S. Mujawar *et al.*, "3D printed Aloe barbadensis loaded alginate-gelatin hydrogel for wound healing and scar reduction: In vitro and in vivo study," *Int. J. Biol. Macromol.*, vol. 296, Mar. 2025, doi: 10.1016/j.ijbiomac.2025.139745.

[17] X. F. Zheng, Q. Lian, and S. T. LianSong, "Chitosan-gelatin-pectin composite films from polyion-complex hydrogels," *Asian Journal of Chemistry*, vol. 25, no. 10, pp. 5363–5366, Aug. 2013, doi: 10.14233/ajchem.2013.14193.

[18] Q. Zhang, M. Zhang, T. Wang, X. Chen, Q. Li, and X. Zhao, "Preparation of aloe polysaccharide/honey/PVA composite hydrogel: Antibacterial activity and promoting wound healing," *Int. J. Biol. Macromol.*, vol. 211, pp. 249–258, Jun. 2022, doi: 10.1016/j.ijbiomac.2022.05.072.

[19] M. A. Abd Jalil, M. L. Md Isa, U. Azhan, K. A. Khalid, M. A. Barkat, and H. Hadi, "Evaluating the Wound Healing Activity of Fabricated Stingless Bee Honey Hydrogels in an Animal Model," *Journal of Pharmacy*, vol. 5, no. 2, pp. 286–304, Jul. 2025, doi: 10.31436/jop.v5i2.399.

[20] P. Nezhad-Mokhtari *et al.*, "Recent advances in honey-based hydrogels for wound healing applications: Towards natural therapeutics," *J. Drug Deliv. Sci. Technol.*, vol. 66, Dec. 2021, doi: 10.1016/j.jddst.2021.102789.
[21] A. M. B. Ratnayake *et al.*, "Machine Learning-Based Acoustic Analysis of Stingless Bee (Heterotrigona itama) Alarm Signals During Intruder Events," *Agriculture (Switzerland)*, vol. 15, no. 6, Mar. 2025, doi: 10.3390/agriculture15060591.
[22] A. M. B. Ratnayake, H. M. Yasin, A. G. Naim, and P. E. Abas, "Buzzing through Data: Advancing Bee Species Identification with Machine Learning," *Applied System Innovation*, vol. 7, no. 4, Aug. 2024, doi: 10.3390/asi7040062.
[23] A. Ratnayake, H. M. Yasin, A. G. Naim, and P. E. Abas, "Classification of Subspecies of Honey Bees using Convolutional Neural Network," *IEEE Xplore*, pp. 1–6, Dec. 2023, doi: 10.1109/ACIIS59385.2023.10367282.
[24] I. C. Călina, A. Scărișoreanu, M. Demeter, E. Mănăilă, and G. Crăciun, "Strategies for Incorporating Natural Therapeutic Agents into Hydrogel Dressings: Innovations in Wound Healing," *Polymers (Basel).*, vol. 17, no. 23, Dec. 2025, doi: 10.3390/polym17233105.
[25] U. Jain and N. Gupta, "Prominent wound healing properties of indigenous medicines," *Journal of Natural Pharmaceuticals*, vol. 1, no. 1, p. 2, Jan. 2010, doi: 10.4103/2229-5119.73579.
[26] Y. Iqbal *et al.*, "Chitosan-based functional materials combined with plant extract: A promising strategy in the stimulation of wound healing process," *J. Drug Deliv. Sci. Technol.*, vol. 101, Nov. 2024, doi: 10.1016/j.jddst.2024.106314.
[27] T. H. Lee *et al.*, "Comparison of extraction methods of phytochemical compounds from white flower variety of Melastoma malabathricum," *South African Journal of Botany*, vol. 148, pp. 170–179, Aug. 2022, doi: 10.1016/j.sajb.2022.04.026.
[28] D. T. Mareta, U. Santoso, Supriyadi, and W. Setyaningsih, "Optimized ultrasound-assisted extraction for phenolic and antioxidant analysis in purple senggani (Melastoma malabathricum) flowers: Influence of developmental stages," *Food Chemistry Advances*, vol. 7, Jun. 2025, doi: 10.1016/j.focha.2025.100949.
[29] D. P. Ferreira *et al.*, "Toxicity and Anti-inflammatory Effects of Eleutherine bulbosa (Miller) Urb, Ethanolic Extract, in Zebrafish (Danio rerio)," *Antiinflamm. Antiallergy Agents Med. Chem.*, vol. 24, no. 3, pp. 199–214, 2025, doi: 10.2174/0118715230352701241130053455.
[30] A. A. Kamarudin, N. H. Sayuti, N. Saad, N. A. A. Razak, and N. M. Esa, "Induction of apoptosis by Eleutherine bulbosa (Mill.) Urb. bulb extracted under optimised extraction condition on human retinoblastoma cancer cells (WERI-Rb-1)," *J. Ethnopharmacol.*, vol. 284, Feb. 2022, doi: 10.1016/j.jep.2021.114770.
[31] M. Ahda, I. Jaswir, A. Khatib, Q. U. Ahmed, and S. N. A. Syed Mohamad, "A review on Cosmos caudatus as A potential medicinal plant based on pharmacognosy, phytochemistry, and pharmacological activities," *Int. J. Food Prop.*, vol. 26, no. 1, pp. 344–358, Jan. 2023, doi: 10.1080/10942912.2022.2158862.
[32] S. H. Cheng, M. Y. Barakatun-Nisak, J. Anthony, and A. Ismail, "Potential medicinal benefits of Cosmos caudatus (Ulam Raja): A scoping review," *Journal of Research in Medical Sciences*, vol. 20, no. 10, pp. 1000–1006, Oct. 2015, doi: 10.4103/1735-1995.172796.
[33] M. Krishani, J. N. Chong, W. R. Lim, N. Jusoh, N. S. Sambudi, and H. Suhaimi, "Synthesis and Characterization of Keratin-Based Scaffold for Potential Tissue Engineering Applications," *Fibers*, vol. 13, no. 7, Jul. 2025, doi: 10.3390/fib13070097.
[34] D. K. Hassan, H. Suhaimi, M. R. Bilad, and P. E. Abas, "Automated Cell Counting using Image Processing," *International Journal of Computing*, vol. 22, no. 3, pp. 302–310, Oct. 2023, doi: 10.47839/ijc.22.3.3224.
[35] L. Zamora-Mendoza, S. N. Vispo, L. De Lima, J. R. Mora, A. Machado, and F. Alexis, "Hydrogel for the Controlled Delivery of Bioactive Components from Extracts of Eupatorium glutinosum Lam. Leaves," *Molecules*, vol. 28, no. 4, Feb. 2023, doi: 10.3390/molecules28041591.
[36] I. L. Lixandru Matei *et al.*, "RETINOL DISPERSION IN THE FORM OF HYDROGEL FOR DERMAL DELIVERY," *Studia Universitatis Babes-Bolyai Chemia*, vol. 2025, no. 2, pp. 37–51, 2025, doi: 10.24193/subbchem.2025.2.03.
[37] A. Kawee-ai, "Advancing Gel Systems with Natural Extracts: Antioxidant, Antimicrobial Applications, and Sustainable Innovations," *Gels*, vol. 11, no. 2, Feb. 2025, doi: 10.3390/gels11020125.